# Variable dispersivity in a column experiment containing $MnO_2$ and FeOOH-coated sand

C.A.J. Appelo [a,b,*], D. Postma [a]

[a] *Department of Geology and Geotechnical Engineering and Groundwater Research Centre, Building 204, Technical University of Denmark, DK 2800 Lyngby, Denmark*
[b] *Hydrochemical Consultant, Valeriusstraat 11, 1071 MB, Amsterdam, Netherlands*

## Abstract

Birnessite ($\delta$-$MnO_2$) has swelling properties that resemble those of clay minerals. If birnessite is present in a sediment, its swelling or shrinking may affect the dispersivity of the sediment. To study the physical behavior of birnessite, a column packed with birnessite-coated sand was injected with a sequence of $CaCl_2$, $MgCl_2$, $FeCl_2$ and KBr solutions. The dispersivity of the sediment as a function of the solution composition was evaluated from breakthrough curves. The birnessite-coated sediment showed in the Mg-form a 4–8 times higher dispersion than in the Ca-form. This is related to differences in swelling behavior observed with X-ray diffraction at 0% relative humidity. After reduction of $\delta$-$MnO_2$ with $FeCl_2$ and precipitation of $Fe(OH)_3$, the dispersion is 10–15 times higher than in the original sediment in the Ca-form. © 1999 Elsevier Science B.V. All rights reserved.

*Keywords:* Reactive transport; Dispersivity; Column experiment; Birnessite; Modeling

## 1. Introduction

In reactive transport modeling, dispersivity is generally treated as a nonvariant physical property of the sediment. However, in some cases, the chemical interactions between the solution and the sediment may change the dispersivity in the course of the reaction. Such interactions may comprise dissolution of minerals present in the sediment or the precipitation of new minerals. Furthermore, the physical properties of minerals

--------

* Corresponding author. Tel.: +31-20-6716366; E-mail: appt@xs4all.nl

may change, for example, due to the swelling behavior of clay minerals (Dufey et al., 1982; Beekman, 1991). The column experiments reported in this contribution indicate that birnessite ($\delta$-$MnO_2$) has properties comparable to clay minerals, such as montmorillonite, with exchangeable cations causing a swelling or shrinking that result in changes in dispersion.

Birnessite is an ubiquitous constituent of soils (Jones and Milne, 1956; Chukrov and Gorshkov, 1981; McKenzie, 1989) and of manganese nodules in marine sediments (Burns and Burns, 1977). It can be synthesized in the laboratory via a variety of pathways (Giovanoli et al., 1970a; McKenzie, 1971; Strobel and Charenton, 1986), and its behavior can thus be studied in the ideal form. It has a large cation exchange capacity that is specific for different ions and varies strongly with pH (Murray, 1975; Tsuji et al., 1992). Therefore, it plays a major role in the behavior of trace metals in natural environments (McKenzie, 1980; Stollenwerk, 1994; Larsen and Postma, 1997). Birnessite has a layer structure consisting of layers of Mn in octahedral coordination with oxygen. The layers have a charge deficit which is compensated by interlayer cations. Depending on the cation and the ambient conditions, a variable amount of water can be incorporated in the structure (Golden et al., 1987; Paterson et al., 1994).

The behavior of birnessite and its effect on dispersion was studied in a column experiment containing natural sand coated with birnessite in which solutions of $CaCl_2$ and $MgCl_2$ of various concentrations were injected. The associated exchange reactions have also been modeled but these results are reported elsewhere (Appelo and Postma, 1999).

Furthermore, birnessite readily participates in redox reactions and is easily reduced by ferrous iron (Hem, 1978; Postma, 1985; Golden et al., 1986). A ferrous iron solution was also injected in the column containing birnessite-coated sand and the following overall reaction did proceed:

$$2Fe^{2+} + MnO_2 + 2H_2O \rightarrow 2FeOOH + Mn^{2+} + 2H^+. \tag{1}$$

In this reaction, the Mn-oxide is dissolved from the sediment, while a Fe-oxide is precipitated. The details concerning the redox processes and their interaction with exchange reactions are again reported elsewhere (Postma and Appelo, 1999). However, the dissolution of Mn-oxide followed by the precipitation of Fe-oxide has a considerable effect on the dispersion properties of the column sediment. The dispersivity of the final column containing FeOOH was assessed by elution with a KBr solution.

## 2. Structure of birnessite ($\delta$-$MnO_2$)

The crystal size of birnessite is generally too small to permit an exact structure refinement. However, various evidence shows that the basic layout of birnessite is similar to the structure of the natural mineral chalcophanite (Giovanoli et al., 1970a; Post and Veblen, 1990; Drits et al., 1997). Chalcophanite, $Zn_2[Mn_6 \square O_{14}] \cdot 6H_2O$, consists of layers of edge sharing $MnO_6$ octahedra which alternate with a layer of water molecules (Wadsley, 1955; Post and Appleman, 1988). One out of seven of the $Mn^{4+}$

positions is empty, which gives a layer charge that is compensated by two Zn atoms located above and below the vacancy (Fig. 1). A structure refinement of $Na_4[Mn_6 \square O_{14}]$ shows the same arrangement of the octahedral layer, but now two Na atoms are located midway between the octahedral layers instead of one Zn atom close to the layer (Chang and Jansen, 1985). In this synthetic $Na_4[Mn_6 \square O_{14}]$ the interlayer water is absent.

The layer charge of chalcophanite is $-2/7 = -0.286$ per $O_2$. Replacement of $Mn^{4+}$ by $Mn^{3+}$ can create additional layer charge, to give a maximum of ca. $-0.33$ per $O_2$ in birnessite (Strobel et al., 1987; Drits et al., 1997). In fact, Post and Veblen (1990) and Drits et al. (1997) found that vacancies were almost absent in their synthetic Na-birnessites, and all the layer charge thus originated from replacement of $Mn^{4+}$ by $Mn^{3+}$. Both the degree of oxidation of Mn and the layer charge are influenced by the way of preparing the birnessite (Bricker, 1965; Giovanoli et al., 1970a,b; McKenzie, 1971; Murray, 1974). Preparations based on $MnO_4^-$ solutions yield more oxidized birnessite with an O/Mn > 1.90. Balistrieri and Murray (1982) found an O/Mn ratio of 1.96 in



Fig. 1. The structure of chalcophanite (after Wadsley, 1955): projection along b-axis (top) and along c-axis (bottom). Reproduced from Strobel et al. (1987).

their sample, and ion exchange is then mainly due to the presence of vacancies. Other preparations, which start with a $Mn(OH)_2$ solution or with solid $Mn_3O_4$ (Bricker, 1965), yield initially a mixed $Mn^{3+}/Mn^{4+}$ compound in which $Mn^{4+}$ can be enriched by washings with acid. Acid attacks $Mn^{3+}$ that is in a relatively weak structural position due to Jahn-Teller distortion. The $Mn^{3+}$ either goes into the interlayer, becomes oxidized, or disproportionates to $Mn^{4+}$ and $Mn^{2+}$ (Giovanoli et al., 1970b; Silvester et al., 1997). The disproportionation of two $Mn^{3+}$ atoms to $Mn^{4+}$ and $Mn^{2+}$ creates a vacancy in the octahedral layer, while $Mn^{2+}$ goes into solution, or into the interlayer.

The *c*-axis spacing of birnessite is 7 or 10 Å, with respectively one or two layers of water molecules in the interlayer region. The amount of water present varies for different interlayer cations and also depends on the ambient conditions (temperature, humidity; Kuma et al., 1994; Paterson et al., 1994). Na-birnessite (buserite) has a 10 Å spacing in water, which decreases to 7 Å upon drying. The process of contraction and expansion is reversible, although after numerous cycles, the water uptake tends to become incomplete (Giovanoli et al., 1970a). Other alkalis likewise give a 7 Å structure upon drying while $Mg^{2+}$, $Ca^{2+}$ and $Ni^{2+}$ forms maintain the 10 Å spacing (Golden et al., 1987; Kuma et al., 1994; le Goff et al., 1996). Transition metal cations can also stabilize a 10 Å spacing (Giovanoli et al., 1975; Golden et al., 1987). At elevated temperature, the structure of Mg- and Ca-birnessite collapses to 7 Å during drying (Golden et al., 1986; Kuma et al., 1994). Post and Veblen (1990) also noted a 7 Å spacing for Mg birnessite when immersed in alcohol. Kuma et al. (1994) have tried to relate the expandability to the ionic radius and hydration energy of the interlayer cation, but the relations are not clear perhaps because the exchange was incomplete. Birnessite is able to absorb alkyl-ammonium ions, and shows similar expansion as vermiculite (Golden et al., 1986). On the other hand, $Na^+$ expands smectites while divalent cations contract the structure, which is commonly related to electrostatic repulsion and hydration energy of the interlayer cation. This behavior is contrary to that of (dried) phyllomanganates, but the difference may well be related to an even more delicate dependency of the latter on ambient humidity. Paterson et al. (1994) observed that when measured wet both Na- and Ca-birnessite maintained the 10 Å spacing, while in the presence of $K^+$ and $Ba^{2+}$ the structure contracted to 7 Å.

## 3. Materials and methods

Mn-oxide-coated sand was collected from a groundwater fed small lake in a gravel pit near Ikast, Denmark. Black Mn-oxide-coated sand was formed at the water table and was apparently the result of in situ oxidation. The sand consists of grains with an average diameter of 0.24 mm covered with a uniform, but friable, blackish brown coating. X-ray diffraction of the coating material showed clear reflections at 2.44 and 1.42 Å and a broad band at 7.5 Å, corresponding to random-stacked birnessite (Giovanoli, 1980). EDAX analysis revealed the following composition: 2.36% $Al_2O_3$, 86.98% $MnO_2$, 7.00% CaO and 3.65% $SiO_2$. The oxidation state of manganese in the coating was determined, using the method of Murray et al. (1984), which yielded an

O/Mn ratio of $1.77 \pm 0.01$. If besides Mn(IV), only Mn(III) is present, this would correspond to a Mn oxide containing 54% Mn(IV) and 46% Mn(III). Coating material was equilibrated with $CaCl_2$ or $MgCl_2$ solutions and XRD measurements at low angles were performed in wet (100% relative humidity) and dry conditions (0% relative humidity in $N_2$ atmosphere). The Ca- and Mg-form exhibited a similar XRD pattern with a peak at 10.0 Å when wet. Upon drying, the Mg-form contracted partly to 9.1 Å, while the Ca-form collapsed to give a broad band from 9 to 7 Å (Fig. 2). The contraction of the Mg-form suggests that about one out of three interlayers has lost one layer of water. The broad band of the dry Ca-form indicates that interlayers have lost one layer of water in a more random fashion.

For the column experiment, the sediment was washed with 0.1 M $Ca(NO_3)_2$ to remove fine particles, with $H_2O$ until the electrical conductivity was 50 μS/cm, and then kept in 10 mM $Ca(NO_3)_2$. The wet sediment was packed in a perspex column of 5.22 cm inner diameter for a length of 5.05 cm. The column was capped by 0.2-cm-thick polyethylene plugs with radial grooves for guiding water from the inlet and to the outlet tubing. To remove gas pockets, the column was drained for water and filled with $CO_2$ gas. When a 10 mM $Ca(NO_3)_2$ solution was pumped into the column, the $CO_2$ was dissolved and all the pores were effectively filled with water. The pore volume was 35.8 ml. In the ensuing experiments, solutions were pumped upward in the column with a Jasco 880-PU HPLC pump at 3 ml/h, and the effluent was sampled with a Gilson 232 sampler.

In the effluent, the concentration of $Fe^{2+}$ was determined spectrophotometrically with Ferrozine (Stookey, 1970) and other cations, Ca, Mg, K, Al, Mn and Fe, by atomic absorption spectrophotometry on acidified samples. Anions, Cl, Br were determined by ion chromatography. pH was measured in a flow cell directly connected to the column outlet.
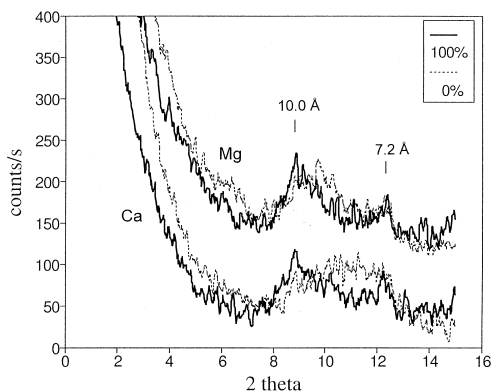


Fig. 2. Low angle X-ray diffraction results of natural birnessite in the $Ca^{2+}$ and $Mg^{2+}$ form at 100% (line) and 0% (dotted line) relative humidity. Cu Kα radiation, 1 s/0.02°.

## 4. Dispersivity in the column experiments

The column pore volume and dispersivity were obtained by least squares optimization of the advection–reaction–dispersion equation (Appelo and Postma, 1993):

$$\frac{\partial C}{\partial t} = -v\frac{\partial C}{\partial x} + D_L\frac{\partial^2 C}{\partial x^2} - \frac{\partial q}{\partial t}, \tag{2}$$

where $C$ is the concentration in water (mol/kg $H_2O$), $t$ is time (s), $v$ is pore water flow velocity (m/s), and $x$ is distance (m). $D_L$ is the hydrodynamic dispersion coefficient (m$^2$/s) $[D_L = D_e + \alpha_L v$ where $D_e$ the effective diffusion coefficient, and $\alpha_L$ is the dispersivity (m)]. $q$ is the concentration in the solid phase (expressed as mol/kg $H_2O$ in the pores). The term $-v(\partial C/\partial x)$ represents advective transport, $D_L(\partial^2 C/\partial x^2)$ gives dispersive transport, and $\partial q/\partial t$ is the change in concentration on the solid ($q$ in the same units as $C$). The usual assumption is that $v$ and $D_L$ are equal for all solute species, so that $C$ can be the total dissolved concentration for a component. For a conservative element, $\partial q/\partial t = 0$.

The solution of Eq. (2) with a flux type boundary condition at the column ends is for a conservative element (van Genuchten, 1981):

$$C(L,t) = C_i + 1/2(C_0 - C_i)A, \tag{3}$$

where $L$ is the column length (m), $C_i$ is the concentration in the resident solution, $C_0$ is the concentration in the injected solution, and:

$$A = \mathrm{erfc}\left(\frac{L - vt}{\sqrt{4D_L t}}\right) + \exp\left(\frac{Lv}{D_L}\right)\mathrm{erfc}\left(\frac{L + vt}{\sqrt{4D_L t}}\right). \tag{4}$$

The dispersivity of the column for the various solution displacements was obtained by a least square fit of Eq. (3) on the different breakthrough curves.

## 5. Results and discussion

The sequence in solution displacements in the column is summarized in Table 1 and the normalized breakthrough curves of the anions for the different experiments are

Table 1
Displacement of column solution in five experiments and dispersivity (mm) optimized from anion break-through curves. Pore volume $V_0 = 35.8$ ml. The pH of the Ca- and Mg- solutions is $5.6 \pm 0.05$

| Exp. | Resident (mM) | Injected (mM) | Dispersivity (mm) |
|---|---|---|---|
| 1 | Ca(NO$_3$)$_2$, 10 | MgCl$_2$, 11 | 1.24 |
| 2 | MgCl$_2$, 11 | MgCl$_2$, 170 | 10.5 |
| 3 | MgCl$_2$, 10 | CaCl$_2$, 50 | 8.2 |
| 4 | CaCl$_2$, 5 | FeCl$_2$, 15 | 2.0 |
| 5 | FeCl$_2$, 15 | KBr, 100 | 20.1[a] |

[a]Optimized with PHREEQC, using mass balance on Br$^-$, $R_{Br} = 1.17$.
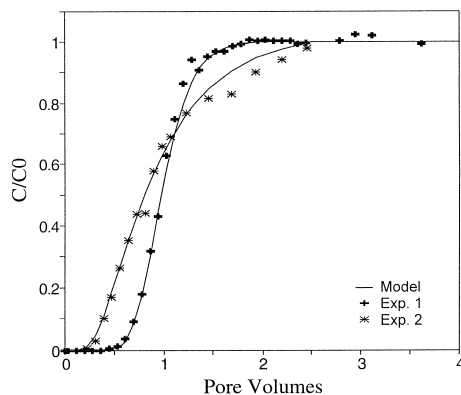
Fig. 3. Normalized breakthrough curves for Cl$^-$ in Exps. 1 and 2 with birnessite-coated sand with fitted curves according to Eq. (3). See Table 1.

shown in Figs. 3–5. Table 1 also contains the dispersivity obtained by the least squares fit of Eq. (3) on the breakthrough curves, with an effective diffusion coefficient $D_e = 0.3 \times 10^{-9}$ m$^2$/s. The pore volume of 35.8 ml was obtained from the first experiment and kept constant in subsequent optimizations.

In the first experiment, a resident 10 mM Ca(NO$_3$)$_2$ solution was displaced from the column with a 11 mM MgCl$_2$ solution. This displacement yielded a dispersivity of 1.24 mm, which may be compared to the average diameter of the sand of 0.24 mm. When in Exp. 2, the 11 mM MgCl$_2$ solution was displaced by a 170 mM MgCl$_2$ solution, the dispersivity increased by a factor of 8 to 10.5 mm. In Exp. 3, a 10 mM MgCl$_2$ was flushed with 50 mM CaCl$_2$ and again a high dispersivity of 8.2 mm was observed. However, in the subsequent experiment (No. 4) where 5 mM Ca$^{2+}$ was displaced with 15 mM FeCl$_2$, a lower dispersivity of 2.0 mm was found, which is close to that in the first experiment. In Exp. 4, the increase of the cation concentration (meq/l) was used
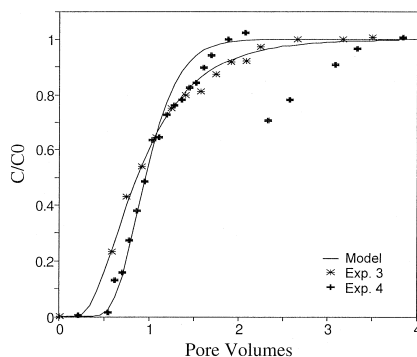


Fig. 4. Normalized breakthrough curves for Cl$^-$ in Exps. 3 and 4 with birnessite-coated sand with fitted curves according to Eq. (3). See Table 1.
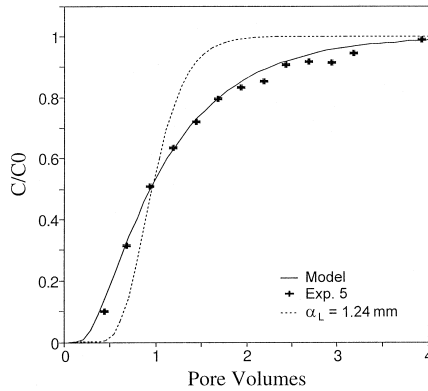
Fig. 5. Normalized breakthrough curves for $Br^-$ in Exp. 5 with $Fe(OH)_3$-coated sand, and a PHREEQC modeled curve according to Eq. (2) with $\alpha_L = 20.1$ mm. For comparison the dotted curve is for $\alpha_L = 1.24$ mm, the dispersivity found in Exp. 1.

for calculating dispersivity, since the anions were not analyzed in the initial part. These results clearly illustrate that the dispersivity of the birnessite-coated sand column is highly dependent on the solution composition.

After a $FeCl_2$ solution was pumped through the column, the birnessite coating on the sediment grains is replaced by a Fe-oxide coating. The dispersivity of the Fe-oxide coating was determined in Exp. 5 by displacement with a 100 mM KBr solution. The $Br^-$ breakthrough showed a retardation of 1.17 and the model breakthrough of $Br^-$ shown in Fig. 5 was obtained with an adapted version of PHREEQC (Parkhurst, 1995), which includes (nonlinear) sorption on $Fe(OH)_3$. The dispersivity of the Fe-oxide-coated sand is 20.1 mm or roughly 10 times larger than the dispersivity of the Ca-birnessite-coated sediment.

Both physical and chemical effects must be considered when discussing the changes in dispersivity. An increased front spreading can be a consequence of increased hydrodynamic instability of the interface of the resident and the displacing solution. It may be induced in upward flow when the displacing solution is less dense (Bachmat and Elrick, 1970; James and Rubin, 1972; Wooding et al., 1997), or in both upward and downward flow when the displacing solution has a lower viscosity (Dullien, 1992). The increased instability of the interface generates fingers which grow with the density and/or the viscosity contrast of the two solutions. Increased front spreading can also be due to anion exclusion which makes the pores less accessible for anions during transport (James and Rubin, 1986). Anion exclusion increases when the anion concentration decreases (Bolt, 1982). Dispersivity has also been observed to increase by a factor of 2 in montmorillonitic soil when the exchangeable sodium percentage increased from 0 to 20% (Dufey et al., 1982). This behavior was related to swelling of clay minerals and blocking of pores for mobile water.

In our experiments, the dispersivity of the birnessite-coated sand could appear to be a function of the salt concentration of the displacing solution (Table 1). However, since the more saline, and hence more viscous fluids, were pumped upwards in the column,

the density and viscosity contrast over the front is expected to decrease dispersion which is the reverse of what is observed. Therefore, the changes in dispersivity of the $MnO_2$-coated sand must be related to changes in the pore structure. The dispersivities listed in Table 1 are derived from the anion breakthrough curves. During transport in the column, the cation and the anion of the injected solution rapidly separate since the injected cation is retarded by ion exchange. The dispersivity of the sediment must then be determined by the resident cation.

In the $Mg^{2+}$ form, birnessite-coated sand shows a higher dispersivity than in the $Ca^{2+}$ form, which implies that $Mg^{2+}$ has the same effect on birnessite as $Na^+$ has on montmorillonite. Swelling of birnessite, which covers the sand grains and forms the contact points, partially blocks pores which then are bypassed by the flowing water. The step change in the concentration of $Cl^-$ arrives therefore earlier at the end of the column. The blocked pores remain accessible by diffusion and the concentration front is therefore smeared out. However, front spreading can still be characterized with the advection–dispersion equation using an increased dispersion coefficient. A simulation with the dual porosity model in CXTFIT (Toride et al., 1995) indicates that when using the small dispersivity of 1.24 mm for the pores through which water flows, the more dispersed profile can be obtained if about half of the pores have become stagnant.

Some signs of stagnancy are apparent in the breakthrough curves. In the second experiment (high $MgCl_2$ injected in Mg-sediment, Fig. 3) chloride levels off early in the tail and cannot be modeled well with the standard advection–dispersion equation. This indicates that stagnant zones have developed in the column. The following displacement with $CaCl_2$ (Exp. 3, Fig. 4) shows the same dispersivity but with less tailing in the end, which indicates that the stagnant zones are disappearing. This may be related to the onset of magnesium displacement from the exchanger sites by calcium. The subsequent displacement of $CaCl_2$ with $FeCl_2$ (Exp. 5, Fig. 4) shows again a small dispersivity initially, but with $C/C_0 > 0.6$ deviations occur. The deviations are probably due to the chemical reactions in the column when $\delta$-$MnO_2$ is reduced by $Fe^{2+}$ and $Fe(OH)_3$ precipitates.

The effects of $Mg^{2+}$ and $Ca^{2+}$ on swelling of the birnessite are apparent. Both the $Ca^{2+}$ and the $Mg^{2+}$ form have an identical *c*-axis spacing of 10.0 Å, but they only behave differently in XRD when humidity is reduced to zero (Fig. 2). How the different behavior in the column experiment must be related to the swelling behavior at 100% humidity is not clear. In any case, the results suggests that dispersivity is extremely sensitive to the detailed behavior of layer minerals as a function of changes in chemical composition of the solution.

The final displacement of $FeCl_2$ with 100 mM KBr showed a much increased dispersivity (Exp. 5, Fig. 5), but is in this case related to changes in the pore structure in the sediment due to the dissolution of birnessite and the precipitation of $Fe(OH)_3$. Note in Fig. 5 that the breakthrough volume for $Br^-$ is much larger than for $Cl^-$ in the previous experiments. It was assumed that the pore volume in the column was not affected by the reaction. When 7.2 mmol $MnO_{1.75}$ dissolves, and 10.7 mmol $Fe(OH)_3$ precipitates, the difference in volume between the precipitated and dissolved mineral is probably in the order of 0.1 ml. This is much less than the total pore volume of 35.8 ml. The exact pore volume could no longer be derived from the breakthrough curve of the

anions, since the precipitated $Fe(OH)_3$ acted as an anion exchanger at the pH of 3.0 in the column. The breakthrough of $Br^-$ and the dispersivity was therefore optimized by modeling with PHREEQC (Appelo and Postma, 1999).

The changes of sediment dispersivity in conjunction with changes in exchangeable cations or dissolution and precipitation of minerals have a bearing on the modeling of the breakthrough curves. The effect will be most conspicuous for conservative or linearly retarded solutes. The breakthrough of solutes which take part in mineral reactions, or which exhibit nonlinear exchange isotherms may be dominated by the reaction term $\partial q / \partial t$ in the advection–reaction–dispersion equation (Appelo, 1996). Since the exact response of dispersivity to exchanger composition can only be speculative at the present stage, the only viable modeling scheme seems to be to take a constant dispersivity value for one displacement experiment, given by the effluent curve of the conservative tracer.

## 6. Conclusions

Birnessite ($\delta$-$MnO_2$) is a layer mineral which exhibits swelling and shrinking due to gains and losses of interlayer water. The swelling depends on the type of interlayer cation, and is intricately connected with column dispersion. Birnessite-coated sediment shows a 4–8 times higher dispersivity in the Mg-form than in the Ca-form. The contrast is related to differences in swelling behavior observed at 0% relative humidity of the Mg- and the Ca-forms. The dispersivity contrast is a factor 2 larger than has been reported for montmorillonitic soil. The enhanced effect is probably due to the nature of the sediment. The grains are coated by the birnessite, and this mineral constitutes the contact points of the individual grains. Even very small swelling effects are therefore important.

The birnessite can be reduced completely with $FeCl_2$ solution. The resulting $Fe(OH)_3$-coated sediment shows at least 10 times higher dispersion than the birnessite-coated sediment in the Ca-form. It is clear that the chemical reactions induce changes in the pore structure, which influence the flow properties of the sediment. Such effects are hitherto not considered in hydrogeochemical transport models.

## References

Appelo, C.A.J., 1996. Multicomponent ion exchange and chromatography in natural systems. In: Lichtner, P.C., Steefel, C.I., Oelkers, E.H. (Eds.), Reviews in Mineralogy, 34, 193–227.
Appelo, C.A.J., Postma, D., 1993. Geochemistry, Groundwater and Pollution. Balkema, Rotterdam, 536 pp.

Appelo, C.A.J., Postma, D., 1999. A consistent model for surface complexation on birnessite $(\delta\text{-}MnO_2)$ and its application to a column experiment. Geochim. Cosmochim. Acta, in press.

Bachmat, Y., Elrick, D.E., 1970. Hydrodynamic instability of miscible fluids in a vertical porous column. Water Resour. Res. 6, 156–171.

Balistrieri, L.S., Murray, J.W., 1982. The surface chemistry of $\delta MnO_2$ in major ion seawater. Geochim. Cosmochim. Acta 46, 1041–1052.

Beekman, H.E., 1991. Ion chromatography of fresh- and seawater intrusion. PhD thesis, Free University, Amsterdam, 198 pp.

Bolt, G.H. (Ed.), 1982. Soil Chemistry: B. Physico-Chemical Models. Elsevier, Amsterdam, 527 pp.

Bricker, O., 1965. Some stability relations in the system $Mn-O_2-H_2O$ at $25°C$ and one atmosphere total pressure. Am. Mineral. 50, 1296–1354.

Burns, R.G., Burns, V.M., 1977. The mineralogy and crystal chemistry of deep-sea manganese nodules, a polymetallic resource of the twenty-first century. Philos. Trans. R. Soc. London, Ser. A 286, 283–301.

Chang, F.M., Jansen, M., 1985. Darstellung und Kristallstruktur von $Na_2Mn_3O_7$. Z. Anorg. Allg. Chem. 531, 177–182.

Chukrov, F.V., Gorshkov, A.I., 1981. Iron and manganese oxide minerals in soils. Trans. R. Soc. Edinburgh 72, 195–200.

Drits, V.A., Silvester, E., Gorshkov, A.I., Manceau, A., 1997. Structure of synthetic monoclinic Na-rich birnessite and hexagonal birnessite: I. Results from X-ray diffraction and selected-area electron diffraction. Am. Mineral. 82, 946–961.

Dufey, J.E., Sheta, T.H., Gobran, G.R., Laudelout, H., 1982. Dispersion of chloride, sodium, and calcium ions in soils affected by exchangeable sodium. Soil Sci. Soc. Am. J. 46, 47–50.

Dullien, F.A.L., 1992. Porous media. Fluid Transport and Pore Structure, 2nd edn. Academic Press, San Diego, CA, 574 pp.

Giovanoli, R., 1980. Vernadite is random stacked birnessite. Miner. Deposita 15, 251–253.

Giovanoli, R., Stähli, E., Feitknecht, W., 1970a. Über Oxidhydroxide des vierwertigen Mangans mit Schichtengitter: 1. Natriummangan(II,III)manganat(IV). Helv. Chim. Acta 53, 209–220.

Giovanoli, R., Stähli, E., Feitknecht, W., 1970b. Über Oxidhydroxide des vierwertigen Mangans mit Schichtengitter: 2. Mangan(III)–manganat(IV). Helv. Chim. Acta 53, 453–464.

Giovanoli, R., Bürki, P., Giuffredi, M., Stumm, W., 1975. Layer structured manganese oxide hydroxides: IV. The buserite group; structure stabilization by transition elements. Chimia 29, 517–520.

Golden, D.C., Dixon, J.B., Chen, C.C., 1986. Ion exchange, thermal transformations, and oxidizing properties of Birnessite. Clays Clay Miner. 34, 511–520.

Golden, D.C., Chen, C.C., Dixon, J.B., 1987. Transformation of birnessite to buserite, todorikite, and manganite under mild hydrothermal treatment. Clays Clay Miner. 35, 271–280.

Hem, J.D., 1978. Redox processes at surfaces of manganese oxide and their effects on aqueous metal ions. Chem. Geol. 21, 199–218.

James, R.V., Rubin, J., 1972. Accounting for apparatus-induced dispersion in analyses of miscible displacement experiments. Water Resour. Res. 3, 717–721.

James, R.V., Rubin, J., 1986. Transport of chloride ion in a water-unsaturated soil exhibiting anion exclusion. Soil Sci. Soc. Am. J. 50, 1142–1149.

Jones, L.H.P., Milne, A.A., 1956. Birnessite, a new manganese oxide mineral from Aberdeenshire, Scotland. Mineral. Mag. 31, 283–288.

Kuma, K., Usui, A., Paplawsky, W., Gedulin, B., Arrhenius, G., 1994. Crystal structures of synthetic 7 Å and 10 Å mangantes substituted by mono- and divalent cations. Mineral. Mag. 58, 425–447.

Larsen, F., Postma, D., 1997. Nickel mobilization in a groundwater well field; release by pyrite oxidation and desorption by Mn-oxides. Environ. Sci. Technol. 31, 2589–2595.

le Goff, P., Baffier, N., Bach, S., Pereira-Ramos, J.P., 1996. Synthesis, ion exchange and electrochemical properties of lamellar phyllomanganates of the birnessite group. Mater. Res. Bull. 31, 63–75.

McKenzie, R.M., 1971. The synthesis of birnessite, cryptomelane, and some other oxides and hydroxides of manganese. Mineral. Mag. 38, 493–502.

McKenzie, R.M., 1980. The adsorption of lead and other heavy metals on oxides of manganese and iron. Aust. J. Soil Res. 18, 61–73.

McKenzie, R.M., 1989. Manganese oxides and hydroxides. In: Dixon, J.B., Weed, S.B. (Eds.), Minerals in Soil Environments. Soil Sci. Soc. Am., Madison, WI, pp. 439–465.

Murray, J.W., 1974. The surface chemistry of hydrous manganese dioxide. J. Coll. Interf. Sci. 46, 357–371.

Murray, J.W., 1975. The interaction of metal ions at the manganese dioxide–solution interface. Geochim. Cosmochim. Acta 39, 505–519.

Murray, J.W., Balistrieri, L.S., Paul, B., 1984. The oxidation state of manganese in marine sediments and ferromanganese nodules. Geochim. Cosmochim. Acta 48, 1237–1247.

Parkhurst, D.L., 1995. User's guide to PHREEQC — a computer program for speciation, reaction-path, advective-transport, and inverse geochemical calculations. US Geol. Surv. Water Resour. Inv. Rep. 95-4227, 143 pp.

Paterson, E., Swaffield, R., Clark, L., 1994. The influence of structure on Ba and K uptake by a synthetic phyllomanganate. Clay Miner. 29, 215–222.

Post, J.E., Appleman, D.E., 1988. Chalcophanite, $ZnMn_3O_7 \cdot 3H_2O$: new crystal-structure determinations. Am. Mineral. 73, 1401–1404.

Post, J.E., Veblen, D.R., 1990. Crystal structure determinations of synthetic sodium, magnesium, and potassium birnessite using TEM and the Rietveld method. Am. Mineral. 75, 477–489.

Postma, D., 1985. Concentration of Mn and separation from Fe in sediments: I. Kinetics and stoichiometry of the reaction between birnessite and dissolved Fe(II) at 10°C. Geochim. Cosmochim. Acta 49, 1023–1033.

Postma, D., Appelo, C.A.J., 1999. Reduction of Mn-oxides by ferrous iron in a flow system: column experiments and reactive transport modeling. Geochim. Cosmochim. Acta, submitted.

Silvester, E., Manceau, A., Drits, V.A., 1997. Structure of synthetic monoclinic Na-rich birnessite and hexagonal birnessite: II. Results from chemical studies and EXAFS spectroscopy. Am. Mineral. 82, 962–978.

Stollenwerk, K.G., 1994. Geochemical interactions between constituents in acidic groundwater and alluvium in an aquifer near Globe, Arizona. Appl. Geochem. 9, 353–369.

Stookey, L.L., 1970. Ferrozine — a new spectrophotometric reagent for iron. Anal. Chem. 42, 779–781.

Strobel, P., Charenton, J.-C., 1986. Influence of foreign cations on the synthesis of various non-stoichiometric forms of manganese dioxide. Rev. Chim. Miner. 23, 125–137.

Strobel, P., Charenton, J.-C., Lenglet, M., 1987. Structural chemistry of phyllomanganates: experimental evidence and structural models. Rev. Chim. Miner. 24, 199–220.

Toride, N., Leij, F.J., van Genuchten, M.T., 1995. The CXTFIT code for estimating transport parameters from laboratory or field tracer experiments, version 2.0. Res. Rep. 137, US Salinity Lab., Riverside, CA.

Tsuji, M., Komarneni, S., Tamaura, Y., Abe, M., 1992. Cation exchange properties of a layered manganic acid. Mater. Res. Bull. 27, 741–751.

van Genuchten, M.Th., 1981. Analytical solutions for chemical transport with simultaneous adsorption, zero-order production and first-order decay. J. Hydrol. 49, 213–233.

Wadsley, A.D., 1955. The crystal structure of Chalcophanite, $ZnMn_3O_7 \cdot 3H_2O$. Acta Crystallogr. 8, 165–172.

Wooding, R.A., Tyler, S.W., White, I., 1997. Convection in groundwater below an evaporating salt lake: 1. Onset of instability. Water Resour. Res. 33, 1199–1217.